

Low-frequency observations of giant pulses from ordinary pulsars

A. N. Kazantsev^{1*}; M. Yu. Basalaeva²,

¹P. N. Lebedev Physical Institute of the Russian Academy of Sciences,
Pushchino Radio Astronomy Observatory, Pushchino 142290, Russia

² Astrophysical school Traektoria,
107078, Moscow, Russia

Abstract

We present our results of investigation of the rate of emission of the giant radio pulses (GRPs) from several second period pulsars, observed with Large Phased Array radio telescope of Pushchino Radio Astronomy Observatory at 111 MHz. It was found that for all pulsars detected rate was not constant and changed with time significantly. Abrupt jumps in the rate of GRPs generation were detected for PSR B0950+08 and PSR B1112+50. We found that GRPs of all pulsars have demonstrated very different clustering properties. Finally, we have carried out the phase analysis of the time of arrival for GRPs and detected their phase with reference to the averaged pulse time of arrival.

1 Introduction

The vast majority of radio pulsars show small pulse-to-pulse intensity variations within the limits of 10 times of the intensity of averaged pulse. However, some pulsars demonstrate unpredictable short-duration outbursts of pulsed radio emission. These pulses were named Giant Radio Pulses (GRPs).

At the present day, only several about 16 pulsars are known to be GRP emitters [1–14], i.e. emit individual pulses that satisfy GRP criteria. These pulsars can be divided into two groups: pulsars with strong magnetic fields at their light cylinders (over $B_{LC} > 10^5$ Gauss) and millisecond periods (including B0531+21, Crab) and ordinary pulsars with B_{LC} from several to several hundred Gauss. Well-known representatives of the former group are Crab pulsar [1] and millisecond pulsar B1937+21 [2]. There are a lot of theoretical models, concerning GRPs from bright, fast-rotating pulsars of the first group [15–18] but much less is known about pulses from the ordinary pulsars with GRPs.

*E-mail:kaz.prao@bk.ru (ANK)

Table 1: Parameters of Pulsars.

Pulsar name epoch 2000(1950)	RAJ (J2000)	DECJ (J2000)	P s	dP/dt s/s	DM $\text{cm}^{-3} \text{ pc}$	PEpoch MJD
J0304+1932 (B0301+19)	03h04m33.115s	19°32'51.4''	1.3876	1.29E-15	15.66	49289.00
J0814+7429 (B0809+74)	08h14m59.50s	74°29'05.70''	1.2922	1.68E-16	5.75	49162.00
J0953+0755 (B0950+08)	09h53m9.3097s	07°55'35.75''	0.2531	2.297E-16	2.97	46375.00
J1115+5030 (B1112+50)	11h15m38.400s	50°30'12.29''	1.6564	2.49E-15	9.19	49334.00
J1136+1551 (B1133+16)	11h36m3.1198s	15°51'14.183''	1.1879	3.73E-15	4.84	46407.00
J1239+2453 (B1237+25)	12h39m40.4614s	24°53'49.29''	1.3824	9.6E-16	9.25	46531.00

Still, we consider that studies of GRPs from the second period pulsars are equally important for the full understanding of pulse generation mechanism. In early work [19] we analyzed the energy characteristics of this group of pulsars. However, we have not studied temporal properties of GRP generation. This issue is clearly very important, because it can shed light on the dynamical behavior of GRPs generation mechanism.

Here we present a statistical study of rate of GRP emission from six pulsars: B0301+19, B0809+74, B0950+08, B1112+50, B1133+16 and B1237+25. Although PSR B0809+74 is not usually considered to be a GRP source, it was reported that it sometimes emitted pulses with anomalous intensity [20] and this emission could be akin to GRPs phenomenon.

The article has the following structure: in Section 2 we describe the process of obtaining data and methods of data analysis, Section 3 contains the results of the analysis for each pulsar. Discussion and conclusions are presented in Section 4 and Section 5 respectively.

2 Observations and data processing

Our observations were made with The Large Phased Array transit radio telescope of Pushchino Radio Astronomy Observatory (LPA LPI) of Astro Space Center, P.N.Lebedev Physical Institute. This is a low-frequency radio telescope with central frequency equal to 111 MHz, and effective bandwidth equal to 2.3 MHz. During our observation sessions, the telescope effective area was $20\,000 \pm 1300 \text{ m}^2$ in the zenith direction. The Single linear polarization was used. For the majority of observations we used the sampling interval 1.2288 ms. The pulsars can be observed only during their culmination when they cross the beam of the LPA LPI. As a result, the duration of observations depends on the declination of a pulsar. For example, the duration of observations of PSR B0809+74 is equal to 11 minutes, and PSR B1237+25 - 3.5 minutes.

Our data processing pipeline can be described as follows. The digital receiver get phased analog signal from the radio telescope. After that, using the synchronizer that generates trigger pulses, the signal is split into a sequence of segments with the duration equal to a period of a given pulsar. The synchro-

nizer has ± 100 ns accuracy when converting GPS time to the universal time scale and ± 10 ns accuracy when setting the start time of the receiver. These accuracies exceeds any reasonable requirements for accuracy of observations at the central frequency of LPA LPI.

The signal is digitized at a frequency of 5 MHz for each pulse. The digitized pulse is accumulated in the receiver's buffer. After digitization, all readings for given pulsar are loaded into the fast Fourier transform hardware processor from the buffer. The processor returns digitized signal as a raw-file observation. The file consists of a header with common information (name of pulsar, start time of observation, time sample, etc.) and array of time-series spectra. Data of time-series spectra are recorded as 32-bit floating-point numbers.

This algorithm does not include absolute calibration of intensity. Thus, units of intensity are analog-to-digital converter (ADC) units.

The next stage of data processing is offline de-dispersion procedure. The de-dispersion process is done at a fixed DM for a given pulsar (see Tab. 1). The de-dispersed pulses for a given observation are saved for subsequent analysis.

For each session of observation, the dynamic average pulse of pulsar is built by summing individual pulses from the observation. The individual pulse is considered to be a giant radio pulse if its peak flux density exceeds the peak flux density of dynamic average pulse by 30 times or more. For each detected GRP the next parametrs were calculated:

- Time stamp of first sample (MJD),
- Time of arrival (MJD),
- Number of pulse in the observation (arbitrary units),
- Amplitude of background (ADC units),
- Amplitude of GRP (ADC units),
- STD noise (ADC units),
- Width of pulse at 50% of peak (ms),
- Width of pulse at 10% of peak (ms).

The rate of GRPs generation was calculated in 30 days long bins and normalized to the total durations of observations in corresponding bins. Additionally, we have performed search for clusters of GRPs, trying to detect consecutive pulses with peak flux density satisfying our criteria.

The phase analysis was carried out in several stages. The phase distributions of giant and non-giant pulses by the longitude of the averaged pulse were analyzed at the first stage. The phase was detected simply as a maximum point of individual pulse. During the second stage, the averaged giant radio pulse and the averaged pulse were calculated by summing all detected pulses from

Table 2: Duration of Observations of Each Pulsar.

Pulsar name	Years	Sessions of observations	Total observations time, h
B0301+19	2012-2016	44	2.42
B0809+74	2012-2017	587	16.39
B0950+08	2012-2017	606	32.48
B1112+50	2011-2018	1214	105.85
B1133+16	2013-2018	781	42.98
B1237+25	2012-2018	606	37.92

Table 3: Rate of GPs generation.

Pulsar name	Maximum, min^{-1}	Average, min^{-1}
B0301+19	0.59	0.09
B0809+74	0.03	0.01
B0950+08	3.10	0.51
B1112+50	0.70	0.24
B1133+16	0.30	0.07
B1237+25	0.38	0.07

pulsars. For the calculation of a location, a half-width and amplitude of the average pulses, they were fitted by Gaussian functions. For fitting one component of the average pulse profile the next function was used:

$$f(t) = ae^{-\frac{(t-b)^2}{2\sigma^2}} \quad (1)$$

where: a is the height of the curve's peak, b is the position of the center of the peak and σ is the standard deviation.

The double- or three-component average pulse of the pulsar was fitted by the sum of two or three Gaussian functions respectively.

3 Results

Summarized information about statistical properties of rate of GRPs generation is presented in Tab. 3. Also we separately present information about clustered GRP in Tab. 4. Hereinafter, we provide detailed information about each pulsar..

3.1 PSR B0301+19

PSR B0301+19 demonstrates an unstable rate of GRPs generation (see Fig. 1). The average rate is approximately 5 giant pulses per hour. Around epoch MJD 57000 a leap in the rate of GRPs generation can be seen. The maximal rate reached a value of 35 impulses per hour. For a significant number of sessions, no individual pulses which can be classified as GRPs were detected.

Table 4: Clusters of GRPs. Numbers of detected pairs of GRPs are in the second column, number of instances of clusters with >2 GRPs are in the third column, and in the last column we show the maximal size of the clusters for each pulsar.

Name	2 GRPs	>2 GRPs	Max size of cluster
B0301+19	1	0	2
B0809+74	2	0	2
B0950+08	29	4	3
B1112+50	95	7	4
B1133+16	1	0	2
B1237+25	3	0	2

Only one cluster of GRPs from PSR B0301+19 was detected: two consecutive GRPs were registered at the MJD 57106. Fig. 2 shows this cluster.

Phase distribution of individual pulses from PSR B0301+19 is shown in the Fig. 3. The giant pulses of the pulsar are located along the longitudes of the main components of the average pulse of the pulsar. The GRPs mostly occur during phase interval of the second component rather than the first (n relation of 3 to 1). However, the GRPs from the first component are more concentrated, located in a narrow interval $25.19 \text{ ms} \pm 0.16 \text{ ms}$. The phase distribution of GRPs coinciding with the second component is wider.

The fitting of the averaged GRP and average pulse which includes all registered pulses is shown in the Fig. 4. According to the fitting results, the distance between components of the average pulse is $64.24 \text{ ms} \pm 0.14 \text{ ms}$. The same parameter for averaged GRP is equal to $63.86 \text{ ms} \pm 0.13 \text{ ms}$.

3.2 PSR B0809+74

As we have already mentioned, PSR B0809+74 is usually not considered to be a GRPs emitter. Nevertheless, it sometimes generates individual pulses that exceed the amplitude of the average profile by 30 or more times. The rate of abnormally strong pulse generation is the lowest of studied pulsars (see Fig. 1). As with PSR B0301+19, there are no strong individual pulses in most observation sessions. On average, PSR B0809+74 generates approximately 1 abnormally strong pulse in 4 hours. The maximum detected rate of GRPs generation is 2 pulses per hour.

We find cluster of 2 consecutive strong pulses which were registered at the MJD 56685 (see Fig. 5);

Strong pulses are located in the middle of the longitude of the average pulse (see left panel of Fig. 6). Despite large number of detected strong pulses, the average pulse is highly jagged (see the right panel of Fig. 6).

3.3 PSR B0950+08

PSR B0950+08 showed a very stable GRPs generation rate (see Fig. 1). There are only several 'empty bins' – bins without registered GRPs. The rate of generation varies between from 0.1 min^{-1} and 0.9 min^{-1} with the average value equal to 0.5 min^{-1} or, i.e. 30 GRPs per hour. There is a jump in rate around epoch MJD 56500 where it increased approximately sixfold, up to 180 GRP per hour.

We detected 33 clusters of GRPs from PSR B0950+08. Four of these clusters include 3 consecutive GRPs. The example of one of these groups is presented on Fig. 7. It can be seen that these GRPs are part of even large group of strong pulses, although not all of them have reached the threshold level (30 average profiles).

The average pulse of pulsar B0950+08 is fairly complex (see the right panel of Fig. 8). It includes precursor area (0 - 25 points) and main pulse (25 - 40 points). Most frequently, GRPs are generated on the second component of the main pulse of pulsar. As a result, the shapes of averaged GRP and average pulse are quite different. Still, distribution of GRPs is not too narrow.

3.4 PSR B1112+50

Of all researched pulsars, PSR B1112+50 demonstrates the most stable rate of GRPs generation (see Fig. 1). In particular, this is especially noticeable in the range from epoch MJD 56500 to the last analyzed observation session. This increase in the rate of GRPs generation began in approximately MJD 57350 and lasted around 90 days. This is the longest increase in the rate of GRPs generation registered in our work. At a maximum rate of GRPs generation for this pulsar reached 42 pulses per hour. That should be compared with the average value around 14 pulses per hour.

Also we detected the largest number of clusters from this pulsar – 102. In 7 cases number of GRPs in them exceeded 2 and the largest cluster contained 4 events. In Fig. 9 we show one of the largest cluster registered in MJD 57489. This group was generated only 21 pulsar period after another cluster of GRPs which included 2 pulses. In another case, presented in Fig. 10, clusters of 4 GRPs and 2 GRPs are separated by faint but still clearly visible individual pulse.

The simple gauss-like shape of an average pulse is typical for the pulsar B1112+50. However, there is an asymmetry of the averaged pulse shape (see right panel of Fig. 11). GRPs from B1112+50 are distributed randomly along the average pulse longitude which is wider than the distribution of non-giant pulses. The averaged GRP is 1.4 times narrower than the averaged pulse which included all detected pulses from the pulsar. There is a significant offset between the peak of the averaged GRP and the peak of the average pulse.

3.5 PSR B1133+16

The rate of GRPs generation from B1133+16 is visibly unstable (see Fig. 1). The maximum of the rate generation was 18 GRPs per hour. On average, the pulsar generates around 4 GRPs per 1 hour. But as it for the pulsar B0301+19, there were no detections in numerous sessions.

During large number of observational sessions, the pulsar B1133+16 generated only single cluster of GRPs on MJD 57658 (see Fig. 13).

The pulsar B1133+16 has double-component average pulse (see right panel of Fig. 14). The distribution of non-giant pulses shown that weak pulses can be recorded between the main components of the profile. GRPs were detected on the main components longitudes only. The fitting results have shown that the distance between the main components for the averaged GRP and the average pulse is significantly different (see Fig. 15). For the average pulse, the distance is equal to $30.34 \text{ ms} \pm 0.16 \text{ ms}$ and for averaged GRP the difference is equal to $28.55 \text{ ms} \pm 0.09 \text{ ms}$.

3.6 PSR B1237+25

The pulsar B1237+25 showed a quite unstable GRPs generation rate (see Fig. 1). Giant radio pulses are detected in 70% of the observational sessions. On average PSR B1237+25 generates approximately 4 impulses per 1 hour. The maximum value of the GRPs rate was 22 pulses per hour. We detected 3 clusters of GRPs (see example in Fig. 16).

The average pulse of B1237+25 is very complex and includes five components. Only three of the components (1, 3, and 5) can be reliably identified in one observational session. The sum of numerous individual pulses allowed us to detect all five components of the average pulse. As seen in Fig. 17, the giant radio pulses are emitted on the longitudes of the 1, 3, and 5 components. We detected only one GRP on the 4-th component of the average pulse. For fitting such a complex average pulse, we use the sum of 5 Gaussian functions (see left panel of Fig. 18). According to the results of the fitting, the positions of 1, 3, and 5 components for average pulse are equal to 20.84 ± 0.03 , 52.26 ± 0.35 , and 76.52 ± 1.06 respectively. The shape of averaged GRP is these components only, and we use the sum of 3 Gaussian functions to fit it. The locations of the components of average GRP are $21.39 \text{ ms} \pm 0.02 \text{ ms}$, $52.24 \text{ ms} \pm 0.57 \text{ ms}$ and $76.4 \text{ ms} \pm 0.15 \text{ ms}$.

4 Discussion

The main result of our study is that the rate of GRP generation in all pulsars is not constant (see Fig. 1). One can interpret this finding in several ways. Firstly, it may reflect the instability of mechanism of GRPs generation. However, the emission rate of typical individual pulses is also subject to strong variability. In this way, the detected rate of GRPs may reflect the common nature of pulse emission, both giant and normal.

A small number of the detected GRPs clusters from PSR B0301+19 is likely related to a short time span of observations. The GRP rate will be defined more precisely with increased observational time.

The rates of GRPs generation of the pulsars B1237+25 and B1133+16 are very similar –they have almost the same value of the average rate and the maximum rates are quite close – 18 and 22 GRPs per hour respectively.

Another striking feature of PSR B1112+50 was the longest train of GRPs. At period 1.6564 s (see Tab. 1) duration of emission of this group of giant pulses was approximately 10 seconds. It could mean that the process giving rise to GRPs in the magnetosphere of this pulsar has a lifespan of considerable duration. This is the only pulsar in our study which demonstrated such extraordinary behavior.

For the majority of our pulsars, the GRPs are located on the longitudes of the main component of the average pulse. The averaged GRPs is not significantly shifted in phase with respect to the average pulse, meaning that the GRPs are emitted in the same region as non-giant pulses.

Only for pulsar B1133+16 the distance between the main components for averaged GRP is significantly narrower than that for the average pulse. This may indicate that the GRPs are emitted from slightly different regions than non-giant pulses. More research should be done for this pulsar.

5 Conclusions

It was found that pulsars B0301+19, B050+08, B1112+50, B1133+16, and B1237+25 demonstrate unstable rate of GRPs generation during all time of observations.

Giant radio pulses from these pulsars are distributed along the longitudes of the main components of an average pulse. Abnormally strong pulses from B0809+74 are strictly located in the middle of the average pulse of the pulsar. This fact shows, that such anomalous pulses are formed rather in the core area of the emission region than in the drifting sub-pulse, which forms essentially part of the pulsar's profile.

For pulsars B0301+19, B050+08, B1112+50, and B1237+25 averaged GRP and average pulse have no significant difference by phase. However, the pulsar B1133+16 demonstrated a narrower average pulse for GRPs than for average ordinary pulses.

We have detected a huge pack of giant radio pulses emitted by B1112+50. The pulsar is the only one that emitted more than 3 consecutive GRPs. Moreover, pulsars B0950+08 and B1112+50 demonstrated jumps in the rate of GRPs generation – in a rather short time the rate increased in 6 and 3 times respectively.

In summary, we have shown that the pulsars with very similar parameters demonstrate significant difference in the rate of GRPs generation and GRP clustering.

Acknowledgements

The authors are grateful to program committee PRAO ASC LPI for the time available on LPA LPI. AK acknowledges the support by the Foundation for the Advancement of Theoretical Physics and Mathematics «BASIS» grant 18-1-2-51-1. We acknowledge the Traektoria foundation for for valuable support of this work. We thank our colleagues V. A. Potapov (Pushchino Radio Astronomy Observatory) and M. S. Pshirkov (Sternberg Astronomical Institute) for useful discussions and contributions during the preparation of this paper.

References

- [1] D. H. Staelin and E. C. Reifenstein, III. Pulsating Radio Sources near the Crab Nebula. Science, 162:1481–1483, dec 1968.
- [2] Cordes J. M. Wolszczan, A. and D. R. Stinebring. Millisecond Pulsars, page 63, 1984.
- [3] A. K. Singal. Giant Radio Pulses from Pulsars. Astrophysics and Space Science, 278:61–64, oct 2001.
- [4] A. A. Ershov and A. D. Kuzmin. Detection of Giant Pulses from the Pulsar PSR B1112+50. Astronomy Letters, 29:91–95, feb 2003.
- [5] S. Johnston and Romani R. W. Giant Pulses from PSR B0540-69 in the Large Magellanic Cloud. The Astrophysical Journal, 590:L95–L98, jun 2003.
- [6] B. C. Joshi, M. Kramer, A. G. Lyne, M. A. McLaughlin, and I. H. Stairs. Giant Pulses in Millisecond Pulsars. Proceedings of the International Astronomical Union Symposium, 2018:319 – 320, 2004.
- [7] H. S. et al. Knight. A Search for Giant Pulses from Millisecond Pulsars. The Astrophysical Journal, 625:951–956, jun 2005.
- [8] A. D. Kuzmin and A. A. Ershov. Giant pulses in pulsar PSR B0031-07. Astronomy and Astrophysics, 427:575–579, nov 2004.
- [9] A. A. Ershov and A. D. Kuzmin. Detection of giant pulses in pulsar PSR J1752+2359. Astronomy & Astrophysics, 443(2):593 – 597, nov 2005.
- [10] A. D. Kuzmin and Ershov A. A. Detection of giant radio pulses from the pulsar PSR B0656+14. Astronomy Letters, 32:583–587, sep 2006.
- [11] Altamose D. Li H. Crawford, F. and Lorimer D. R. Variability of the Pulsed Radio Emission from the Large Magellanic Cloud Pulsar PSR J0529-6652. The Astrophysical Journal, 762:8, jan 2013.

- [12] A. N. Kazantsev and V. A. Potapov. Discovery of Giant Pulses from the Pulsar B1237+25(J1239+2453). Astronomicheskii Tsirkulyar, 1620:1–7, jan 2015.
- [13] A. N. Kazantsev and V. A. Potapov. Discovery of Anomalously Strong (Giant) Pulses from the Pulsar B1133+16 (J1136+1551) at a Frequency of 111 MHz. Astronomicheskii Tsirkulyar, 1628:1–8, oct 2015.
- [14] Potapov V. A. Kazantsev, A. N. and G. B. Safronov. Discovery of Anomalous Strong (Giant) Pulses from PSR B0301+19 (J0304+1932) at 111 MHz. Astronomicheskii Tsirkulyar, 1638:1–5, jul 2017.
- [15] T. H. Hankins, J. S. Kern, J. C. Weatherall, and J. A. Ellek. Nanosecond radio bursts from strong plasma turbulence in the Crab pulsar. Nature, 422(6928):141–143, mar 2003.
- [16] Ya. N. Istomin. Origin of Giant Radio Pulses. IAU Symposium, 2018:369 – 372, 2004.
- [17] S. A Petrova. Nature of Giant Pulses in Radio Pulsars. Chinese Journal of Astronomy and Astrophysics, 6(S2):113 – 119, oct 2006.
- [18] G. Machabeli, N. Chkheidze, and I. Malov. Energy accumulation mechanism in pulsar magnetospheric plasma eigen-waves and formation of Giant Radio Pulses. Astrophysics and Space Science, 364(3), mar 2019.
- [19] A. N. Kazantsev and V. A. Potapov. Search for giant pulses of radio pulsars at frequency 111 mhz with lpa radio telescope. Research in Astronomy and Astrophysics, 18(8):97, aug 2018.
- [20] Zakharenko V. V. Konovalenko O. O. Lecacheux A. Rosolen C. Rucker H. O. Ulyanov, O. M. Detection of Individual Pulses from Pulsars B0809+74; B0834+06; B0943+10; B0950+08 and B1133+16 in the Decameter Wavelengths. Radio Physics and Radio Astronomy, 11:113, june 2006.

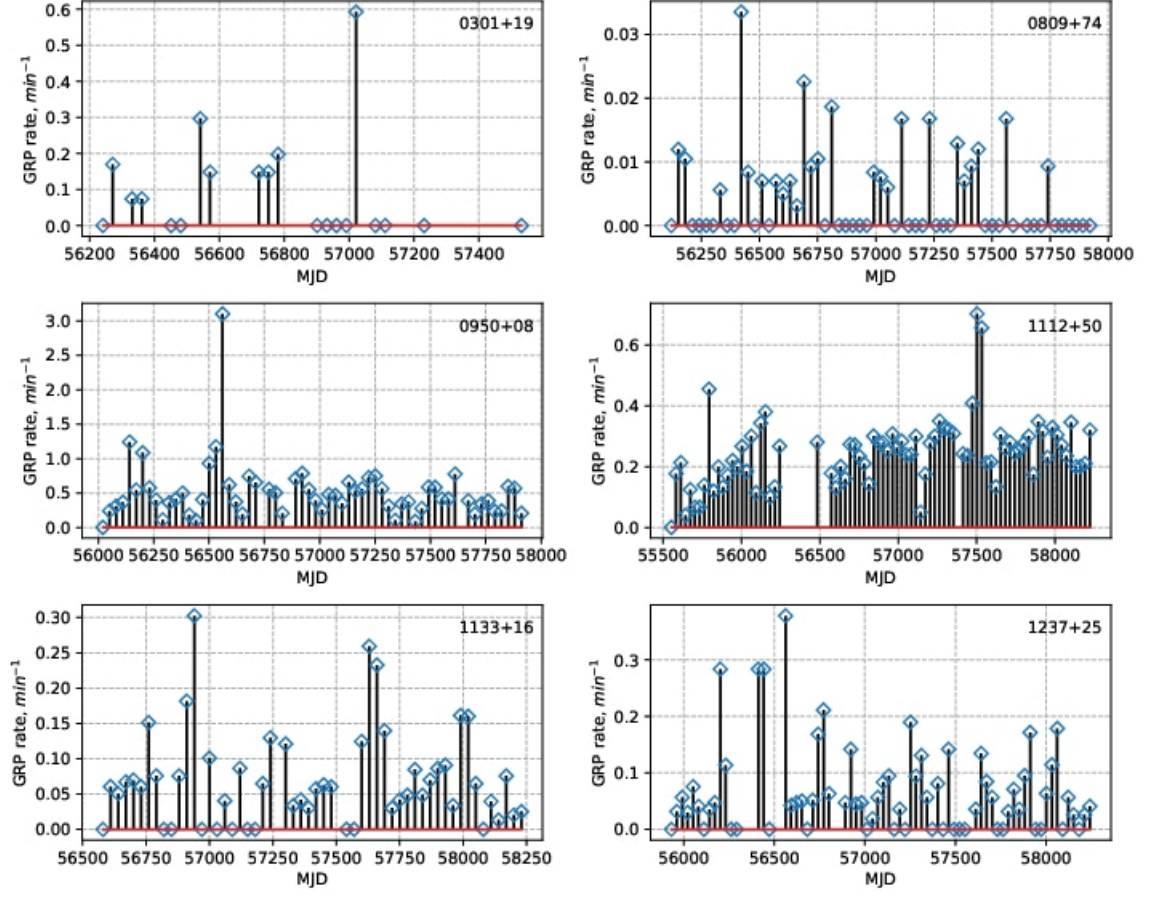


Figure 1: Rate of the emission of GRPs of studied pulsars. Each point contains 30-day averaged data.

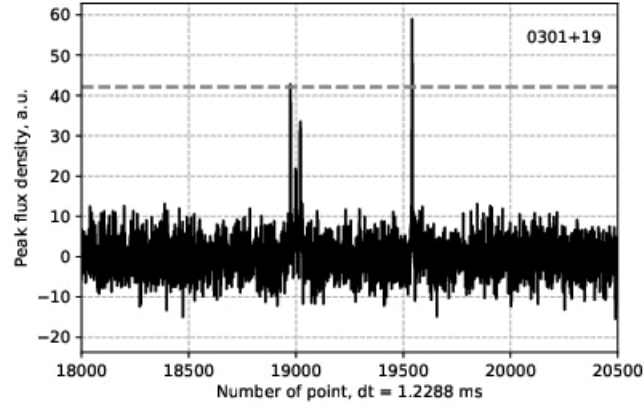


Figure 2: The only group of GRPs detected from B0301+19 at MJD 57106. Gray dashed line shows the 30 peak flux density of dynamic averaged pulse.

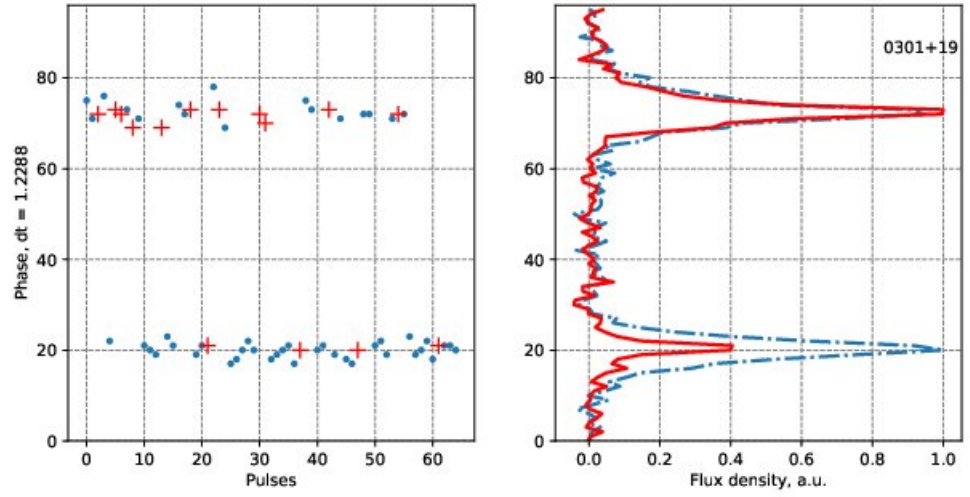


Figure 3: Phase distribution of non-giant (blue points) and giant (red pluses) pulses from B0301+19.

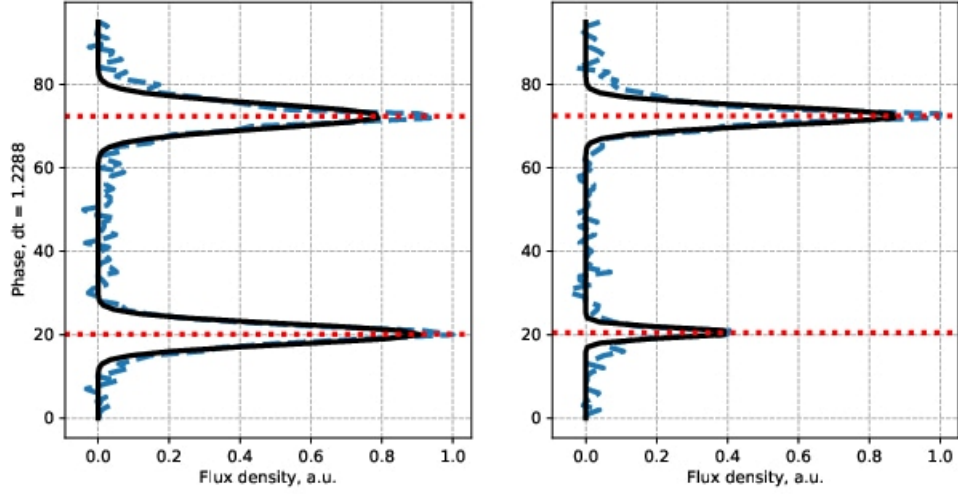


Figure 4: The fitting of the averaged pulse (left panel) and the averaged GRP (right panel) from B0301+19 by sum of 2 Gaussian functions. Red dot lines show an expected value for the first and the second Gaussian function.

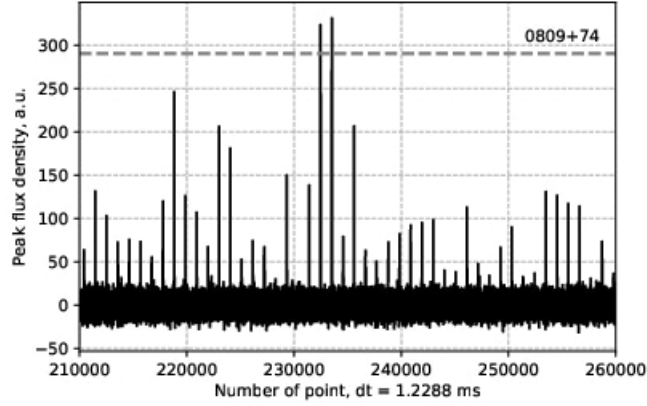


Figure 5: The example of group GRPs detected from B0809+74 in MJD 56685. Gray dashed line shows the 30 peak flux density of dynamic averaged pulse.

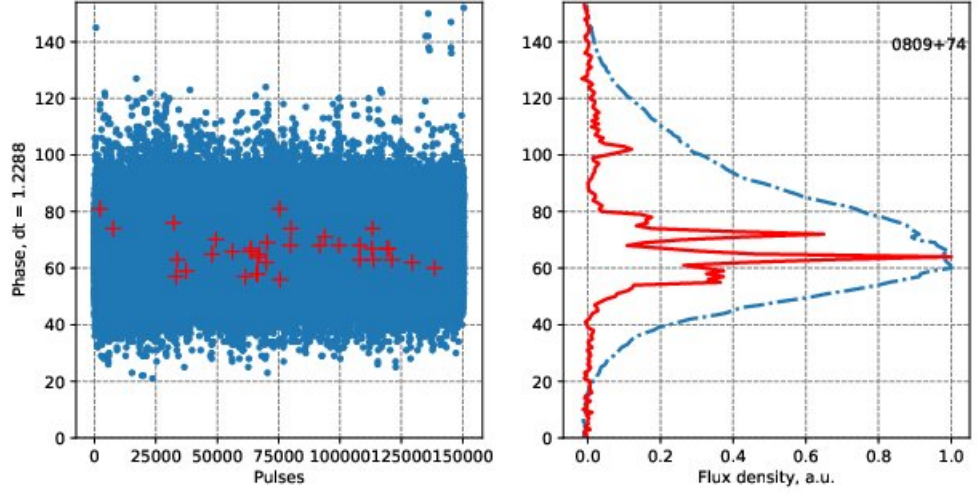


Figure 6: Phase distribution of non-giant (blue points) and abnormally strong (red pluses) pulses from B0809+74.

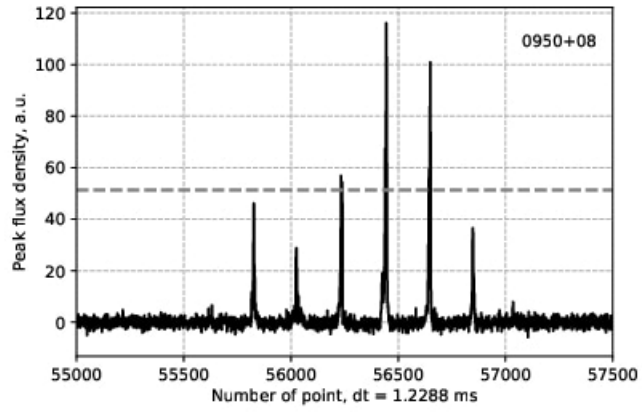


Figure 7: The example if group GRPs detected from B0950+08 in MJD 57476. Gray dashed line shows the 30 peak flux density of dynamic (calculated during current observation session) averaged pulse.

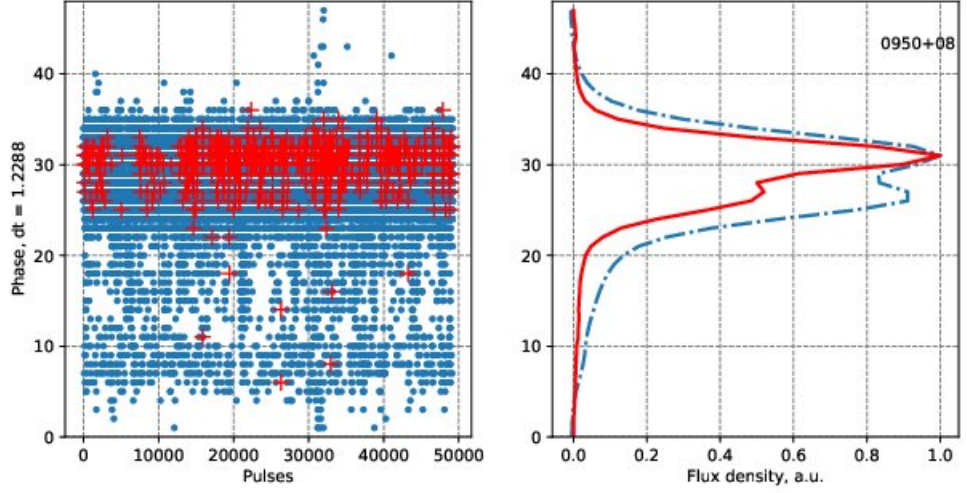


Figure 8: Phase distribution of non-giant (blue points) and giant (red pluses) pulses from B0950+08.

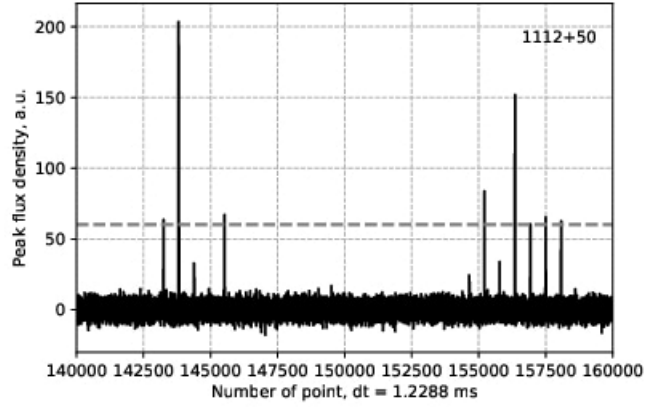


Figure 9: The example of cluster GRPs detected from B1112+50 in MJD 57489. Gray dashed line shows the 30 peak flux density of dynamic averaged pulse.

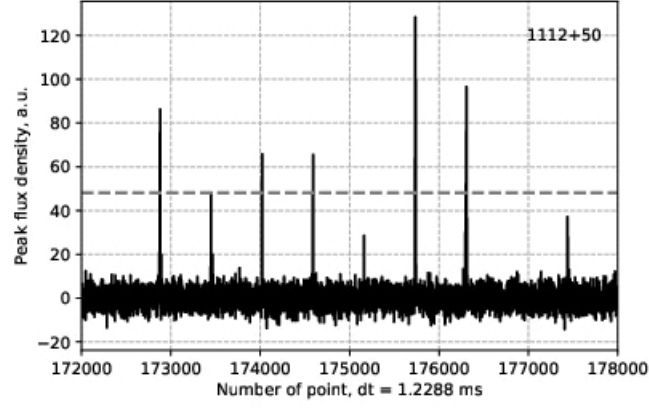


Figure 10: The example of group GRPs detected from B1112+50 in MJD 57515. Gray dashed line shows the 30 peak flux density of dynamic averaged pulse.

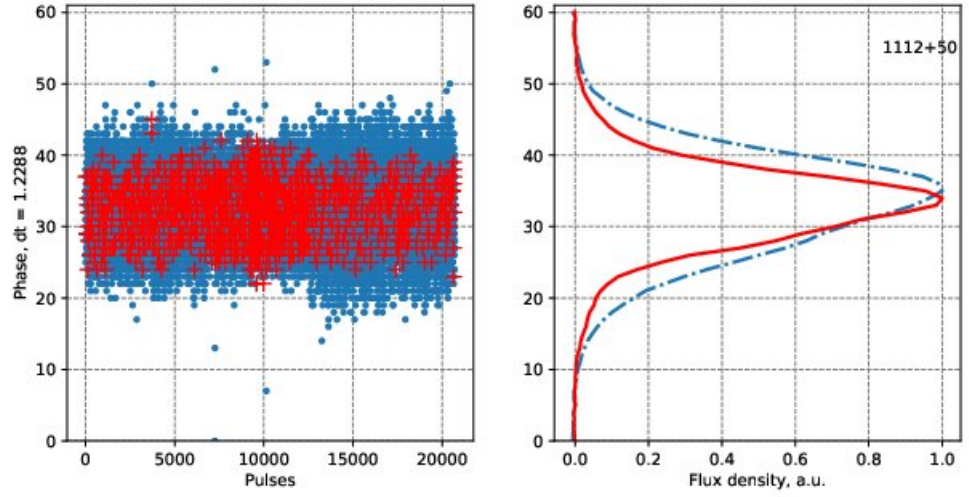


Figure 11: Phase distribution of non-giant (blue points) and giant (red pluses) pulses from B1112+50.

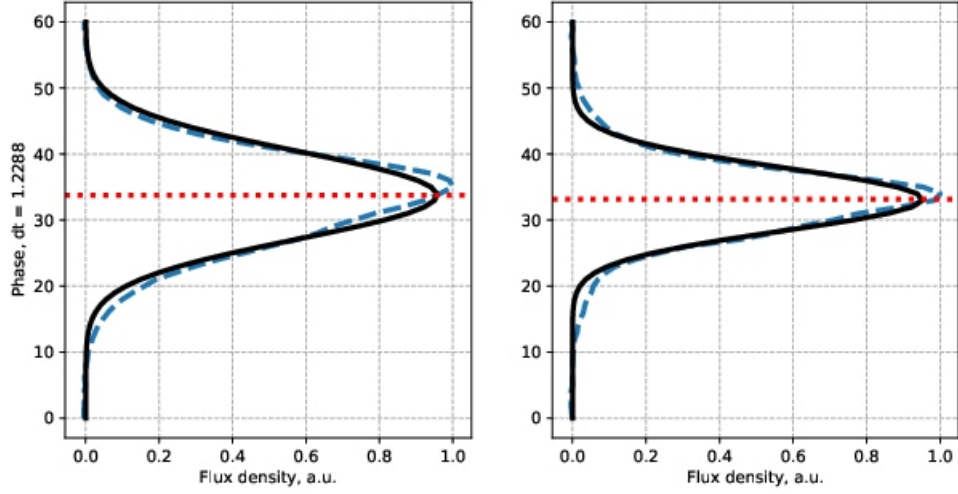


Figure 12: The fitting of the averaged pulse (left panel) and the averaged GRP (right panel) from B1112+50 by Gaussian function. Red dot line shows an expected value for the Gaussian function.

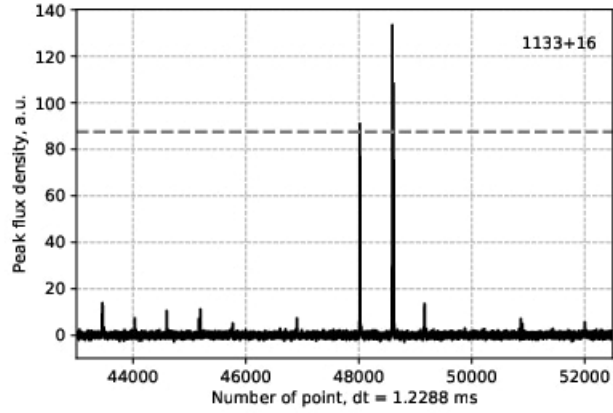


Figure 13: The only cluster of GRPs detected from B1133+16 in MJD 57658. Gray dashed line shows the 30 peak flux density of dynamic averaged pulse.

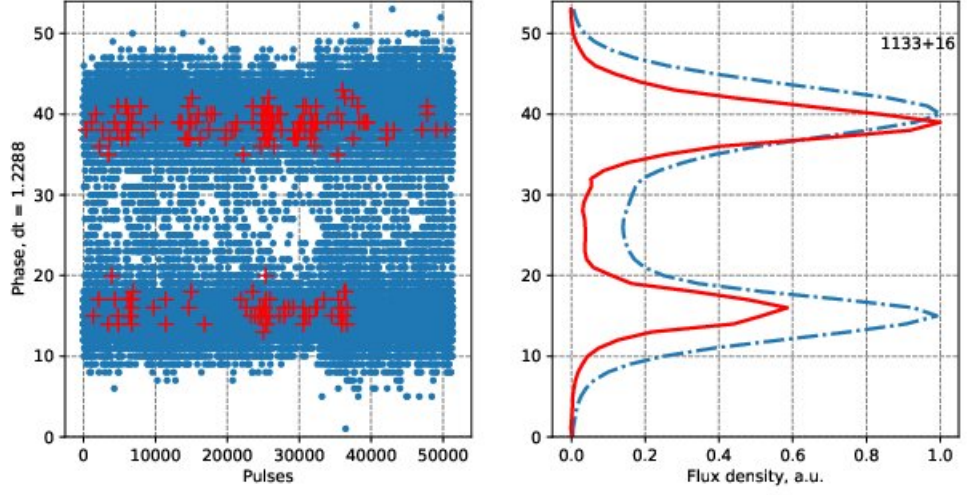


Figure 14: Phase distribution of non-giant (blue points) and giant (red pluses) pulses from B1133+16.

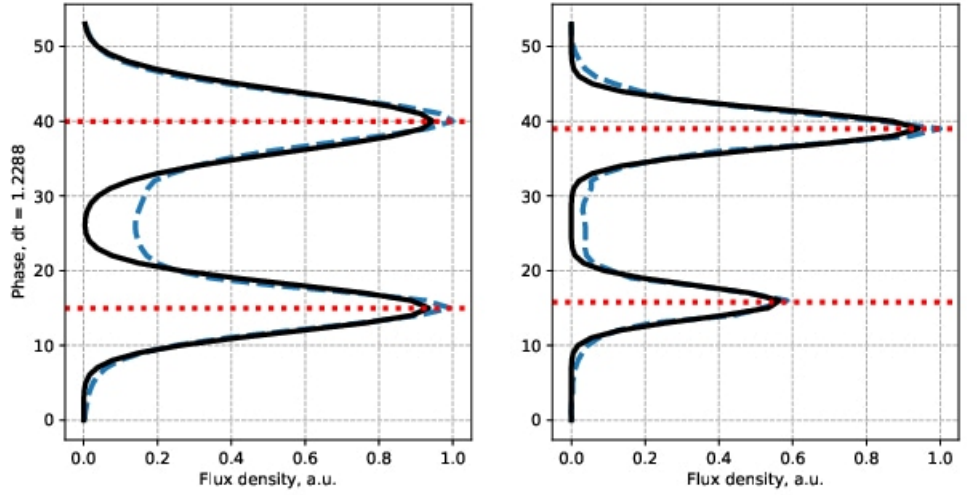


Figure 15: The fitting of the averaged pulse (left panel) and the averaged GRP (right panel) from B1133+16 by sum of 2 Gaussian functions. Red dot lines show an expected value for the first and the second Gaussian function.

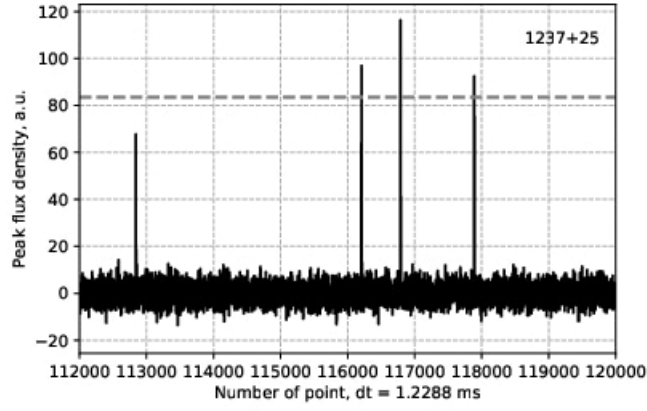


Figure 16: The example of cluster GRPs detected from B1237+25 in MJD 56760. Gray dashed line shows the 30 peak flux density of dynamic averaged pulse.

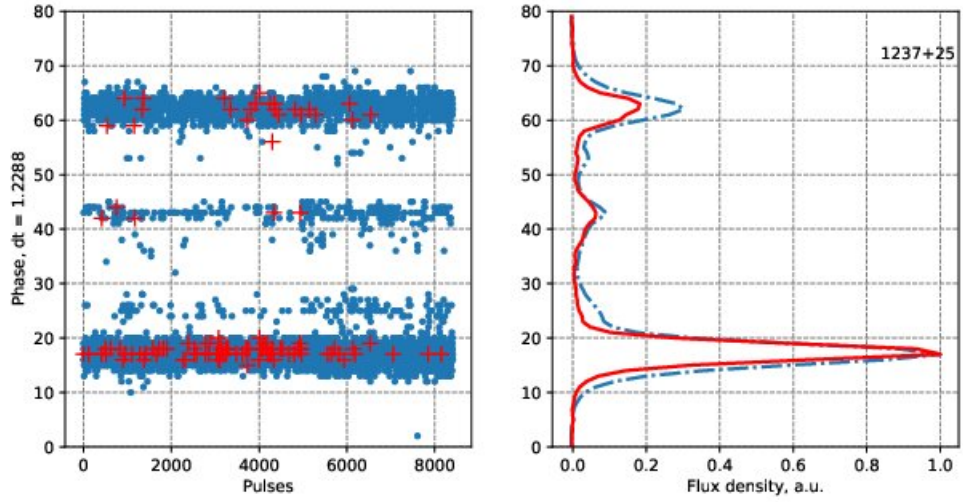


Figure 17: Phase distribution of non-giant (blue points) and giant (red pluses) pulses from B1237+25.

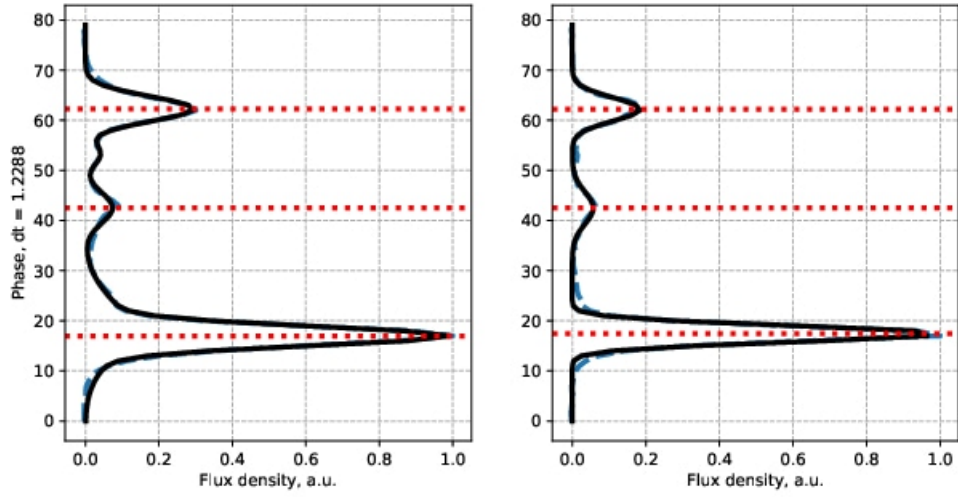


Figure 18: The fitting of the averaged pulse by sum of 5 Gaussian functions (left panel) and the fitting of the averaged GRP by sum of 3 Gaussian functions (right panel) from B1237+25. On the right panel, red dot lines show an expected value for the Gaussian. functions. On the left panel, red dot lines show an expected value for the first, third and fifth Gaussian functions.